CRYSTAL ORIENTATION EFFECTS DURING FABRICATION OF SINGLE OR MULTI-CRYSTAL NB SRF CAVITIES*

D. Baars[#], T.R. Bieler[†], Dept. Chem. Eng. & Mat. Sci.,
A. Zamiri, F. Pourboghrat, Dept. Mech. Eng.,
C. Compton, National Superconducting Laboratory, Michigan State University

Abstract

Single and large-grain Nb SRF cavities are of interest due to possible reduction of cost and problems associated with inconsistent texture and surface finish among batches of rolled polycrystalline Nb sheet. The effect of crystal orientation on dislocation density, surface quality, and recrystallization after plastic deformation and e-beam welding was investigated, as understanding of their interrelations is needed. These were evaluated for three samples of different orientations at steps similar to those in typical cavity forming, with deformation modeled using a crystal plasticity approach. Initial dislocation density was higher than expected, increased with deformation, after welding was reduced in recovered areas, and was similar to initial density in recrystallized grains; there was also evidence that Nb has a higher tolerance for dislocations than other metals. Surface quality depends on a complex relation of crystal orientation, slip system activity, and prior surface treatment. Recrystallization nucleated outside the melt pool, and the new orientations grew both epitaxially into the weld as it solidified, and away until heat and time were insufficient to continue growth.

INTRODUCTION

Manufacturing superconducting radio frequency (SRF) cavities from single crystal niobium is being investigated as an alternative to polycrystalline niobium for several reasons: 1) single crystal sheets may be cut directly from the purified ingot, eliminating the cost of rolling into polycrystalline sheet, 2) polycrystalline sheet texture varies among manufactures and even between batches, leading to variability in forming and surface finish, 3) a single crystal cavity has already been tested and matches the capability of polycrystalline cavities. However, knowledge about the effects of different crystal orientations on dislocation density, surface quality, and recrystallization after plastic deformation and e-beam welding are needed.

Prior work on electron-beam welding showed that it is possible to weld two single crystals together, and achieve a bond line in the middle of the weld [1]. This observation implies that the material surrounding the weld forms the basis for epitaxial solidification as the melt pool solidifies. However, this epitaxial resolidification pattern was disturbed when the weld passed grain boundary on one side, indicating that the presence of three solid-liquid interfaces with different energies affects the orientation of solidifying grains. At some distance from the triple junction, a stable bicrystal weld was re-established.

While this result is encouraging for retaining large crystal configurations in the welding process, this prior experiment was conducted with undeformed single crystal pieces. Thus, an important issue to assess is whether deformed single crystal niobium can be welded together without generating many new crystal orientations. A prior result that investigated a bent single crystal sample deformed to ~14% strain and heated similarly to welding did not recrystallize [1]. However, recrystallization along the weld of a finished large-grain cavity has been observed (Figure 1). A set of single crystal tension specimens were deformed, cut in half, and welded together with a different half.

As surface finish is perhaps the most crucial final outcome of forming a cavity, the cavity is etched to remove a damaged/contaminated layer. As etching preferentially removes material that has defects at a greater rate than material without defects, these experiments also provide the opportunity to assess the effect of surface energy on etching phenomena.

Ultimately, welding and etching depends on the defect state in the metal, so the single crystal properties and microstructures of these specimens are also measured carefully. The deformation is modeled using a crystal plasticity finite element formulation to assist in interpreting measurements. Furthermore, it is known that the defect state can affect the thermal conductivity of the niobium, particularly relative to the 'phonon peak' that occurs at about 2K [2]. Thus, the sequence of single crystal experiments described below intended to simulate the operations that take place during the production of a superconducting radio frequency cavity.
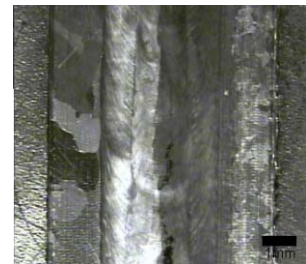
Figure 1. Recrystallization around a finished large grain cavity's equator weld

MATERIALS & METHODS

Single crystal Nb samples were cut from the outer scrap rings that were left over after making a prototype 1.3 GHz, β=0.81 elliptical single cell cavity. Portions of the ring were trimmed into dog-bone shape tensile coupons using electro-discharge machining (EDM). The gage length was 18mm with 1mm fillets at the shoulders,

3.4mm wide, and 2.8mm thick; each grip section length was 10mm, 5mm wide, and 2.8mm thick. Samples were then polished to mirror finish, first mechanically to 0.05μm colloidal silica, and then electropolished using 12V for 8min at -30°C. After orientation imaging microscopy (OIM), three samples with orientations close to (110)[001], (110)[-110], and (111)[-110], i.e. (crystal direction parallel to surface normal of sample)[crystal direction parallel to tensile axis]. These three samples were selected because each had either a surface normal or tensile direction in common with another specimen.

The surface roughness measurements were made along the polished gage length using an optical profiler (WYCO, Veeco Instrument's Vision32 software) to establish a baseline average surface roughness (Ra); each measurement's area was 1.2mm2 and compensated in the software for linear tilt and curvature of the surface. To assess the effect of crystal normal direction on etching of undeformed material, about two-thirds of each sample's gage length was covered with a strippable protective coating (Coscoat 4300, General Chemical Co., Detroit MI) , leaving one-third that was exposed to a 20min buffered-chemical polish (BCP) etch, with no temperature control of the acid. After polishing, the protective coat was removed, and the surface roughness measurements were made along the gage length in both the etched and protected areas.

In anticipation of measuring local strains after tensile testing, a grid was put onto the unpolished back of each sample by spray painting through a wire mesh, and digitally photographed. Each sample was then mounted in a tensile testing machine (Instron 4302, Instron's Bluehill software) with the etched end in the lower stationary clamp and the protected end clamped to the moving crosshead. Each sample was taken to 40% engineering strain, assuming uniform elongation of the gage length. Digital photographs were taken of each distorted grid, and compared with the previous image to estimate local strains.

Surface roughness measurements were made at several locations along the gage length. Each sample was then cut in half with a diamond saw and BCP etched for 10min, with no temperature control of the acid. The halves were bagged in a clean room, and e-beam welded together at Sciaky (Chicago, IL), as indicated in Table I. After welding, surface roughness measurements were made again along the gage length. In order to make OIM measurements possible, the welded samples were then electropolished, using 12V for 10min at -30°C.

OIM scans were done in and adjacent to the weld, at suspected recrystallization fronts, and relatively far from the weld, near the shoulder. Composite inverse pole figure OIM maps were assembled, prisms superposed to show crystal orientation based on the actual sample surface normal, as deformation caused the original surface normal to rotate or twist according to the activated deformation systems.

Several techniques were used to evaluate dislocation density at different processing steps. Electron channeling contrast imaging (ECCI) was used to image initial dislocation density in each sample over several small areas of ~100μm^2. ECCI exploits highly localized rotations of the crystal lattice adjacent to a dislocation. When the beam axis is aligned with a diffraction band edge in a selected area channeling pattern, it is possible to maximize image contrast in the region adjacent to the dislocation, analogous to imaging dislocations in TEM [3]. Since the area examined is necessarily small to image dislocations' contrast (area ~100μm^2), a high density of dislocations generated by deformation complicates interpretation, and this method was not used after deformation except in recrystallized grains. Kernel average misorientation maps highlighted small changes in lattice rotation over larger areas ~4mm^2. These maps are formed by comparing each data point to others 50μm away, and the difference in rotation displayed using a 0° (blue) to 5° (red) gradient scale, highlighting low-angle grain boundaries and shear bands (sheet-like arrangements of dislocations). Finally, synchotron x-ray measurements were made in 1 μm steps along a line parallel to the weld edge on the (110)[-110] side of the (111)[-110]/(110)[-110] sample to examine the internal defect state of two recrystallized grains with a small recovered grain region between them and adjacent to the weld (Argonne National Laboratory, Argonne IL).

A crystal plasticity finite element modeling (CPFEM) approach was used to predict active slip systems, assuming that slip on (110) planes had the lowest critical resolved shear stress (CRSS), with (112) plane slip having a 20% higher CRSS, and (123) slip was not activated. Using an optimization technique, Zamiri et al. showed that during the plastic deformation of a single crystal, the slip rate on any slip system can be obtained by [4]:

$$\dot{\gamma}^\alpha = \lambda \frac{\frac{\text{sign}(\tau^\alpha)}{\tau_y^\alpha} \exp\left(\frac{\rho}{m}\left(\frac{|\tau^\alpha|}{\tau_y^\alpha}-1\right)\right)}{m\sum_{\beta=1}^{N}\exp\left(\frac{\rho}{m}\left(\frac{|\tau^\beta|}{\tau_y^\beta}-1\right)\right)}$$

where m and ρ are materials parameters, λ is a Lagrange multiplier, and τ^α and τ_y^α are resolved shear stress and critical resolved shear stress for slip system α, respectively.

This crystal plasticity model was used to study the activation of the slip systems in high purity niobium. For this purpose, a single 8 noded brick element with unit side was used and uniaxially deformed along Z axis of the reference coordinate system using ABAQUS [5]. The two faces of the cube normal to the axis of loading are constrained to remain parallel to each other throughout the simulation. The simulations were conducted to a final 0.6 strain. Such kind of computational model which simulate the rigid testing machine has been also used by Anand and Kothary[6], and Raphanel et al. [7] for study of the activation of slip systems in different crystals.

The strain hardening model is expressed by the following hardening equation:

$$\dot{\tau}_y^{\alpha} = \sum_{\beta=1}^{N} h^{\alpha\beta} \left| \dot{\gamma}^{\beta} \right|$$

where $\dot{\gamma}^{\beta}$ is the plastic slip rate on the active slip system β and $h^{\alpha\beta}$ are denoted as the components of the hardening matrix. The $h^{\alpha\alpha}$ are known as self-hardening moduli while $h^{\alpha\beta}$ for ($\alpha \neq \beta$) are known as the latent-hardening moduli. Several equations have been proposed for the hardening matrix. Hutchinson [8], Chang and Asaro [9], and Peirce et al.[10] proposed the simple law:

$h^{\alpha\beta} = h^{\beta}[q + (1-q)\delta^{\alpha\beta}]$ (no summation on β).

Here q is the so-called latent-hardening ratio, which is the ratio of the latent-hardening rate to the self-hardening rate of a slip system with values in the range of $1 < q < 1.4$. Parameter q can be considered as 1 for coplanar slip systems and 1.4 for non-coplanar slip systems. h^{β} is an evolutionary function denoting the self-hardening rate, which can be expressed as a function of either shear slips or resolved shear stress on slip systems. h^{β} is considered to evolve as following:

$$h^{\beta} = h_0 \left| 1 - \frac{\tau_y^{\beta}}{\tau_s} \right|^{a} \cdot \text{sign}\left(1 - \frac{\tau_y^{\beta}}{\tau_s} \right)$$

where h_0, a, and τ_s are slip system hardening parameters which are considered to be identical for all slip systems. h_0 denotes the initial hardening rate, τ_s the saturation value of the slip resistance, and a is the exponent describing the shape of the function.
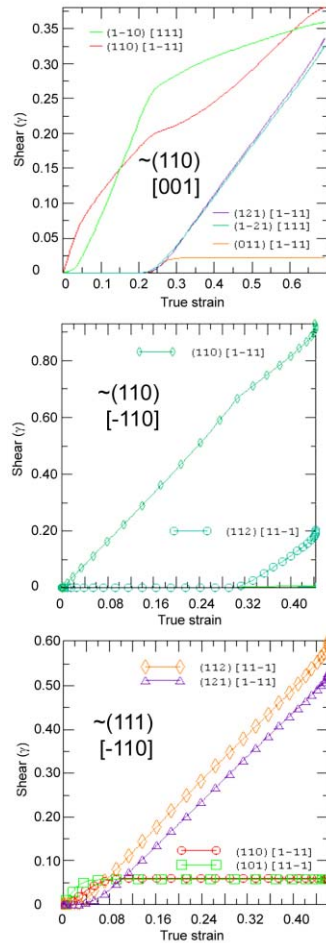
Figure 2. Activity of slip systems used by the crystal plasticity ode during simulated deformation, which depends on each sample's initial crystal orientation (~initial orientation given in larger text).

RESULTS & DISCUSSION

The three orientations used in the experiment exhibited different deformation behaviors when deformed in tension, associated with different combinations of activated slip systems, as indicated in Table I and Figure 2. The composite orientation maps of welded specimens in Figures 3-5 shows that with a strain of about 40%, recrystallization occurred, but the details differed in each specimen. Examination of the associated inverse pole figures shows that the peak spread is greater in the recovered regions than the recrystallized regions, indicating retention of significant low angle boundary/dislocation networks. The surface roughness showed complex interrelationships between surface normal and activated deformation systems, discussed more below.

The three simulations of deformation of the single crystals indicated that the amount of shear on different slip systems depended strongly on the initial crystal orientation, as shown in Figure 2. In one specimen, slip on a single (110) plane was favored until a large strain was reached, and slip on a (112) plane commenced. In the other two specimens, two (110) slip systems were activated nearly equally, but in one case, slip on a pair of (112) planes became more favorable shortly after yielding, while in the other, slip on (112) planes did not commence until significant strain on the pair of (110) slip systems had occurred. Thus, the three specimens have very different populations of dislocations present in the deformed material. Furthermore, the amount of strain in each specimen differed, particularly in one sample where deformation occurred mainly in an area where the cross-section had been reduced by prior BCP etching. Thus each half of the welded specimen had differing amounts of prior strain and dislocation content, as summarized in Table I.

Recrystallization differed in each specimen, according to the crystal orientations and dislocation populations present after deformation. Similar new orientations formed and grew in the heat affected zone of crystals with the same initial orientation (Figure 3).

Table 1. Orientations welded together with Descriptions of Weld Characteristics, Strain, and Recrystallization

Left Initial orientation, Initial BCP	Activated slip systems	Strain at Rx front, Rx trend weld detail	Right Initial orientation, Initial BCP	Activated slip systems	Strain at Rx front, Rx trend weld detail
~(110)[001] Figure 3	2 {110} 2 late {112}	61%, 3mm away (weld blow-through - no weld to grow into)	~(111)[-110] Figure 3	2 Early {110} 2 Majority {112}	27%, 4.4mm away from weld bead
~(110)[-110] Figure 4	Single {110}	21%, 3.5mm away & into weld	~(110)[001] Figure 4	2 {110}	7%, 1.5mm away
~(111)[-110] Figure 5	2 Early {110} 2 Majority {112}	33%, 4.6mm away & into weld	~(110)[-110] Figure 5	Single {110}	40%, 3mm away & into weld

From the inverse pole figure maps in Figure 3, it is evident that while the peaks are sharper in the recrystallized grains, they are not much sharper than the recovered grains. This implies that over the large areas scanned, there are significant orientation gradients even in recrystallized grains, implying that niobium has a rather
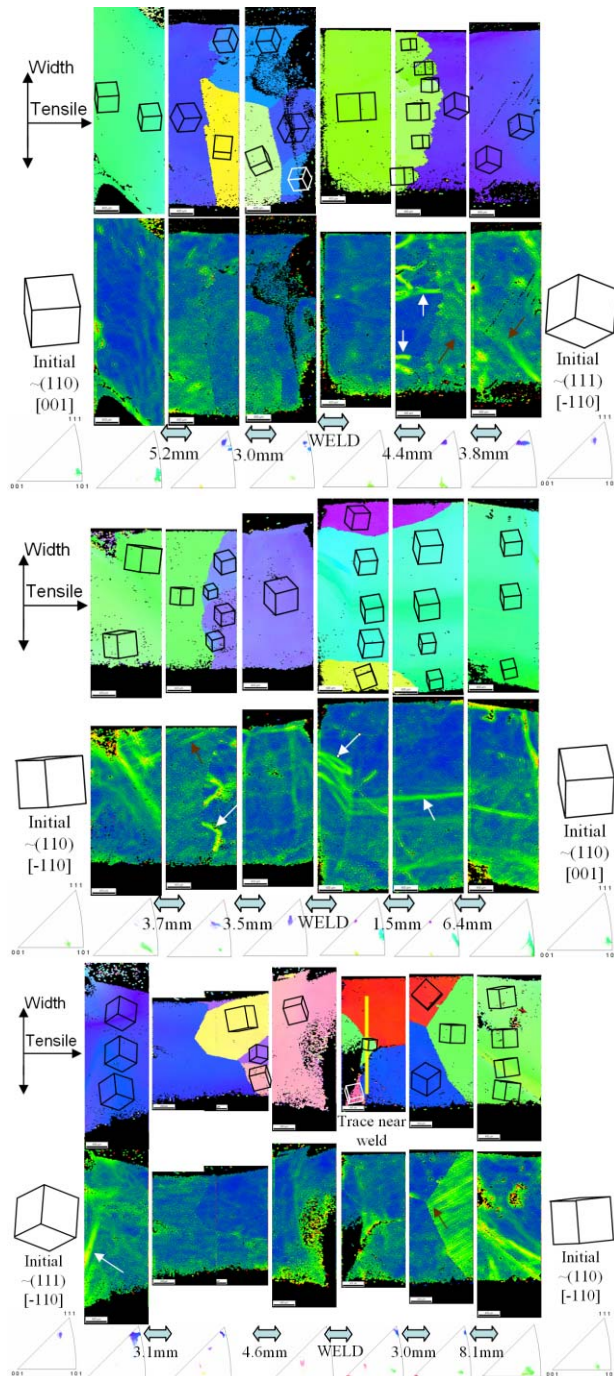
Figure 3 Crystal orientations (normal direction inverse pole figure maps), kernel average misorientation, and discrete point inverse pole figures for the three welded specimens.

high tolerance of dislocations. A sequence of diffraction patterns were taken using synchrotron radiation along a trace just to the right of the weld pool in the (111)[-110]/(110)[-110] specimen. This trace passed the through

two red and blue recrystallized orientations, and a recovered original (green) crystal orientation near the middle of the weld. The synchrotron diffraction patterns had sharp peaks in recrystallized grains as expected, indicating few dislocations within the ~100 μm deep x 2 μm column interrogated by the x-ray beam. Within the recovered region (green grain), the peaks were consistently smeared, indicating significant lattice curvature, and thus high dislocation density (Figure 4). Also, the blue recrystallized grain orientation showed a much deeper penetration of lattice curvature into the grain interior than the red orientation, for reasons that are not clear. That some of the initial high dislocation density persisted despite being adjacent to the melt pool also suggests that niobium has a high tolerance for dislocations.
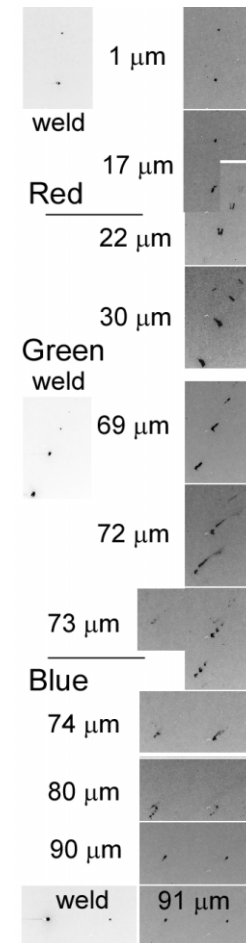
Figure 4 Synchrotron Laue peaks of Rx red, prior green, and Rx blue orientation adjacent to weld in the (110)[-110] and (-110)-[110] sample - note streaked patterns in recovered green grain and subgrains present as far as 15 μm from green-blue grain boundary.

ECCI of as-received single crystal samples (Figure 4) revealed large tangles of dislocations in thick cell walls. Surprisingly, after deformation and welding, recrystallized grains still had significant dislocation content, as compared with other recrystallized metals, Dislocations were distributed uniformly, but in a lower quantity than the as-received specimens. Kernel average misorientation maps show shear bands appearing as bright bands of higher lattice curvature (geometrically necessary dislocation content) that terminated on the recrystallization front (brown arrows). Recrystallized regions show much thicker large sweeping bands of high lattice curvature (white arrows). One reason that may account for this consistent observation of high dislocation content is that the maximum tensile/compressive stress direction is in the most compliant [111] direction of the crystal, suggesting that dislocations in niobium have less stored elastic strain energy in dislocation pileups than other metals. Also, the large thermal gradients associated with solidification of an ingot or a weld may generate significant dislocation content upon cooling.
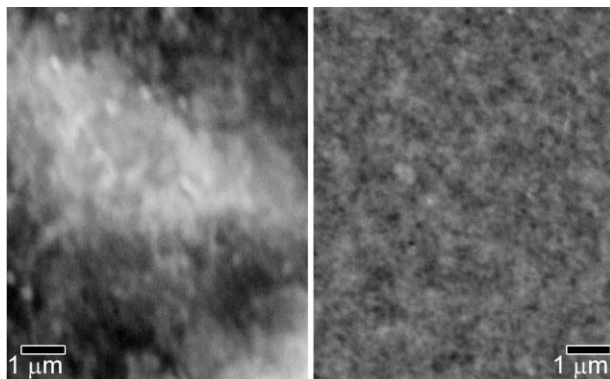
Figure 4 Dislocations imaged with ECCI in as-received ingot (left) and a recrystallized grain near weld (right).
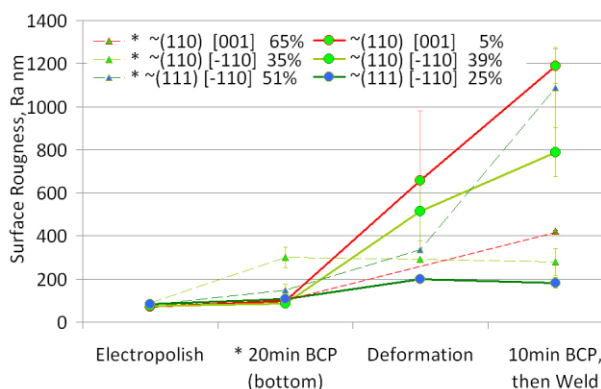
Figure 5 Surface roughness at various process stages.

The changes in surface roughness with sequential process steps is shown in Figure 5 (note only half of the specimens experienced the 20min BCP etch). The initial average surface roughness (Ra) after EP was similar for all orientations, ~70-80nm. After the 20 minute BCP etch, the Ra of the exposed area doubled for (111)[-110] and tripled for (110)[-110], while (110)[001] increased by half. The protective coatings leaked slightly under their edges, leading to varying Ra increases even in regions labeled 'protected'. After deformation to 40% strain, there was a very large Ra increase in both (110) surface normal samples' protected areas, while the previously etched (110)[-110] area stayed the same (No Ra data for deformed (110)[001]). This trend continued after the 10 minute BCP etch and weld step, with both (110) surface normal samples' protected areas increasing in roughness, while the previously etched areas stayed the same or moderately increased. In contrast, the trend observed for (110) surface normal specimens was reversed for the (111) surface normal sample, as the previously etched area became moderately rougher after deformation and then much rougher after the 10 minute BCP and weld step, while the protected area increased moderately after deformation and remains the same after the 10 minute BCP etch and weld. The relationship between the amount of local strain and Ra is inconclusive. The strongest correlation between the effect of etching on surface roughness is that the majority of slip occurred on {110} planes in samples with a (110) surface normal, whereas

slip on {112} planes was dominant in the (111) surface normal sample. This suggests that the relative amount of activity of various slip systems may have a strong effect on etching behavior, and hence, on Ra.

CONCLUSIONS

Strains similar to those found in typical cavity forming processes are sufficient to initiate recrystallization upon EB welding. Nucleation of new recrystallized grains begins in heated regions on either side of the melt pool, and these new orientations grew epitaxially into the weld as the melt pool solidifies as well as away from the weld toward the shoulder, until there was insufficient heat and time to continue the growth. Recrystallized grains contain larger than expected density of dislocations, though fewer than deformed/recovered regions. Surface roughness depends upon a complex interaction of crystal orientation, slip system activity, and prior surface treatment.

REFERENCES

[1] D. Baars, H. Jiang, T.R. Bieler, C. Compton, T.L. Grimm, Crystal Orientations Near Welds in High RRR Niobium with Large Grains, Applied Superconductivity Conference 2006.

[2] A. Aizaz, T. Grimm, P. Bauer, Performance of Superconducting Radio Frequency Cavities for Accelerators: A Novel Approach to Overcome Thermal Limitations Through Surface Modifications. Applied Superconductivity Conference 2006.

[3] M.A. Crimp, Scanning Electron Microscopy Imaging of Dislocations in Bulk Materials, Using Electron Channeling Contrast, Microscopy Research and Technique. 69:374–381 (2006).

[4] A. Zamiri, F. Pourboghrat, A novel yield surface for single crystals: combined constraints crystal plasticity model. (in preparation).

[5] ABAQUS manual (2002). Hibbit, Karlsson & Sorensen Inc, Providence, RI, Version 6.3.

[6] Anand, L., Kothari, M., 1996. A computational procedure for rate independent crystal plasticity. Journal of the Mechanics and Physics of Solids 44, 525–557.

[7] Raphanel, J.L., Ravichandran, G., Leroy, Y.M., 2004. Three-dimensional rate-dependent crystal plasticity based on Runge–Kutta algorithms for update and consistent linearization. International Journal of Solids and Structures 41, 5995–6021.

[8] Hutchison, J.W., 1976. Elastic–plastic behavior of polycrystalline metals and composites. Proceeding of the Royal Society London, Series A 319, 247–272.

[9] Chang, Y.W., Asaro, R.J., 1981. An experimental study of shear localization in aluminum–copper single crystals. Acta Metallurgica 29, 241.

[10] Peirce, D., Asaro, R., Needleman, A., 1982. An analysis of nonuniform and localized deformation in ductile single crystals. Acta Metallurgica 30, 1087–1119.